



**HAL**  
open science

# A cellular automata-based deterministic inversion algorithm for the characterization of linear structural heterogeneities

P. Fischer, Abderrahim Jardani, N. Lecoq

► **To cite this version:**

P. Fischer, Abderrahim Jardani, N. Lecoq. A cellular automata-based deterministic inversion algorithm for the characterization of linear structural heterogeneities. *Water Resources Research*, 2017, 53 (3), pp.2016-2034. 10.1002/2016WR019572 . hal-01696131

**HAL Id: hal-01696131**

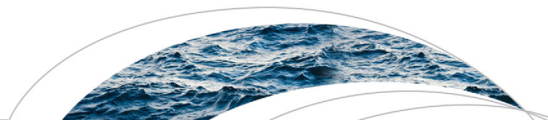
**<https://hal.science/hal-01696131>**

Submitted on 3 Dec 2021

**HAL** is a multi-disciplinary open access archive for the deposit and dissemination of scientific research documents, whether they are published or not. The documents may come from teaching and research institutions in France or abroad, or from public or private research centers.

L'archive ouverte pluridisciplinaire **HAL**, est destinée au dépôt et à la diffusion de documents scientifiques de niveau recherche, publiés ou non, émanant des établissements d'enseignement et de recherche français ou étrangers, des laboratoires publics ou privés.

Copyright



## RESEARCH ARTICLE

10.1002/2016WR019572

### Key Points:

- A novel inverse approach is developed to reconstruct the structural heterogeneities
- The cellular automaton method is used to parameterize the inverse problem
- The inverse algorithm is validated on the hydrogeological and geophysical data

### Correspondence to:

A. Jardani,  
abderrahim.jardani@univ-rouen.fr

### Citation:

Fischer, P., A. Jardani, and N. Lecoq (2017), A cellular automata-based deterministic inversion algorithm for the characterization of linear structural heterogeneities, *Water Resour. Res.*, 53, 2016–2034, doi:10.1002/2016WR019572.

Received 27 JUL 2016

Accepted 11 FEB 2017

Accepted article online 15 FEB 2017

Published online 11 MAR 2017

# A cellular automata-based deterministic inversion algorithm for the characterization of linear structural heterogeneities

P. Fischer<sup>1</sup>, A. Jardani<sup>1</sup>, and N. Lecoq<sup>1</sup>

<sup>1</sup>Normandie Université, UNIROUEN, UNICAEN, CNRS, M2C, Rouen, France

**Abstract** Inverse problem permits to map the subsurface properties from a few observed data. The inverse problem can be physically constrained by a priori information on the property distribution in order to limit the nonuniqueness of the solution. The geostatistical information is often chosen as a priori information; however, when the field properties present a spatial locally distributed high variability, the geostatistical approach becomes inefficient. Therefore, we propose a new method adapted for fields presenting linear structures (such as a fractured field). The Cellular Automata-based Deterministic Inversion (CADI) method is, as far as we know when this paper is produced, the first inversion method which permits a deterministic inversion based on a Bayesian approach and using a dynamic optimization to generate different linear structures iteratively. The model is partitioned in cellular automaton subspaces, each one controlling a different zone of the model. A cellular automata subspace structures the properties of the model in two units (“structure” and “background”) and control their dispensing direction and their values. The partitioning of the model in subspaces permits to monitor a large-scale structural model with only a few pilot-parameters and to generate linear structures with local direction changes. Thereby, the algorithm can easily handle with large-scale structures, and a sensitivity analysis is possible on these structural pilot-parameters, which permits to considerably accelerate the optimization process in order to find the best structural geometry. The algorithm has been successfully tested on simple, to more complex, theoretical models with different inversion techniques by using seismic and hydraulic data.

## 1. Introduction

In geophysics, the inverse method is an efficient way for mapping the geological structures by assessing the physical properties of the subsurface (such as hydraulic conductivity, electrical resistivity, magnetic susceptibility, volumetric density, porosity, etc.) from a set of observed data. These observed data represent the responses of the investigated area to solicitations applied during the geophysical surveys (pumping tests, electrical resistivity tomography, electromagnetic, gravimetry, seismic, etc.). Commonly, the inverse problems are undetermined, with nonuniqueness of the solution, leading to provide doubtful interpretations of the geophysical surveys. Thus, the addition of a priori information on the properties to estimate is a necessity for avoiding the physically unrealistic models. Most often, geostatistical constraints are used to reconstruct the physical properties of a soil that can be modeled by smooth spatial variabilities [Hoeksema and Kitanidis, 1984]. However, when the parameters have a high spatial variability, the use of statistical characteristics as a priori information becomes ineffective and inadequate to locate the discontinuities of the physical properties. Therefore, several algorithms have been proposed to deal with the “structural” inversion, considering both the estimation of physical properties and reconstruction of boundaries between different heterogeneities.

Among these approaches, we cite those which incorporate structural information in the model parameterization of the inverse problem, such as the multiscale method that rests on an increasing resolution of the parameterization during the optimization sequences [Grimstad *et al.*, 2003]. The adaptive multiscale method permits to reduce the number of unknown parameters by a local refinement of the parameterization where the heterogeneity is the most important, to avoid an overparameterization. Tsai *et al.* [2003] used the Voronoi zonation with a pilot-point parameterization method to identify parameters structures in a model.

For the approaches using no specific parameterization of the model, Lelièvre and Oldenburg [2009] have proposed to incorporate constraints to the inversion objective function in terms of some structural information such as orientation to obtain more realistic solutions. The spatial distribution of the unknown parameters

can also be approximated by a sparse set of coefficients to be identified in a compressed sensing sparsity-promoting inversion [Jafarpour *et al.*, 2010] which promotes sparse solutions. Finally, the inversion with total variation prior [Lee and Kitanidis, 2013] uses a Laplace prior instead of a Gaussian in a Bayesian inversion in order to delimitate the shapes of discrete structures piloted by some hyperparameters determined during the inversion using an expectation-maximization approach.

In another register, Lochbühler *et al.* [2015] used the training image method in the inverse formulation to represent the structural characteristics of a field as prior information to eliminate inversion artifact and improve the estimate of the parameters. Hale [2009] and Soueid Ahmed *et al.* [2015] have proposed the guided image method in which the structural features of the domain is presented graphically and used as a priori information to guide the inversion by refining the model sensitivity at boundaries between different zones. It permits a better estimate of the intrastructure parameter variabilities and location of different features in a model. The level set is an alternative approach to detect the interfaces between different facies thanks to the use of extensible boundaries that move during the inversion process to fit the observed data [Lu and Robinson, 2006; Cardiff and Kitanidis, 2009]. Haber and Oldenburg [1997] have identified the profits that could bring joint inversion to structural identification and have presented a protocol to run a joint inversion in geophysics by constraining the results with a unique structural consideration. Since then, several other structural joint inversions tools have been developed which were summarized in a review proposed by Gallardo and Meju [2011]. This review presents the recent techniques of structural joint inversions and the upcoming challenges of such inversions in the next years.

However, regarding the imaging of linear structures, which are characterized by an aperture significantly lower than their length (such as karst conduits and fractures), the deterministic inversion remains, according to our knowledge, an unexplored subject. The inverse modeling of such structures requires a large-scale parameterization, which makes the computation very heavy particularly in the case of stochastic or global optimization algorithms [Pardo-Igúzquiza *et al.*, 2012; Reeves *et al.*, 2013; Bruna *et al.*, 2015; Javadi *et al.*, 2016].

In this paper we propose a new method called Cellular Automata-based Deterministic Inversion (CADI), adapted for the inversion of linear structures. This approach is based on a Bayesian formulation with the use of Cellular Automaton (CA) concept to parameterize the model. The dynamic structural optimization in the algorithm is controlled by the CA, which allows the drive of an entire discretized system with only some local configurable interaction rules. After a global presentation of the model parameterization, we will detail the interaction rules chosen for the CA in this CADI algorithm to reproduce linear structures (section 2.1). Then we will present the structure of the inverse problem (section 2.2) and the protocol of optimization (section 3). Several examples conducted with the CADI algorithm on linear problems (seismic) and nonlinear problems (hydraulic tomography) are described in the last part of this paper (section 4).

## 2. Parameterization of Inverse Problem Using Cellular Automaton

### 2.1. Parameterization of the Model

In the CADI method, the distribution of the properties in the model is structurally generated by several CA. In previous works, CA have already been coupled to global optimization algorithms such as genetic algorithms [Dewri and Chakraborti, 2005; Ghosh *et al.*, 2009]. However, in the CADI method we wanted to couple the possibilities offered by CA to a deterministic inverse process. Therefore, the model (discretized in  $m$  cells) is partitioned in  $m_{CA}$  CA subspaces (with  $m_{CA} \ll m$ ), each one being monitored by an independent CA configured by its neighborhood definition (Figure 1). Thus, the CA subspaces and their parameterization are pilot zones for the model, which permits to avoid an overparameterization of the inverse problem.

The CA is a widely used mathematical system to generate discrete dynamic models. It has been applied to diverse fields of modeling such as Random Number Generators [Tan and Guan, 2007], chemical reactions [Van der Weeën *et al.*, 2011], solid-solid phase transformation during heating [Halder *et al.*, 2014, 2015] or cooling [Dewri and Chakraborti, 2005; Ghosh *et al.*, 2009; Jin and Cui, 2012], fluid flow through fractures [Pan *et al.*, 2011], or transport in fluid flow [Chopard and Masselot, 1999]. The CA is a popular method due to its capacity to model complex systems by using simple rules. In fact, the evolution of the entire system is driven by some configurable local interaction rules.

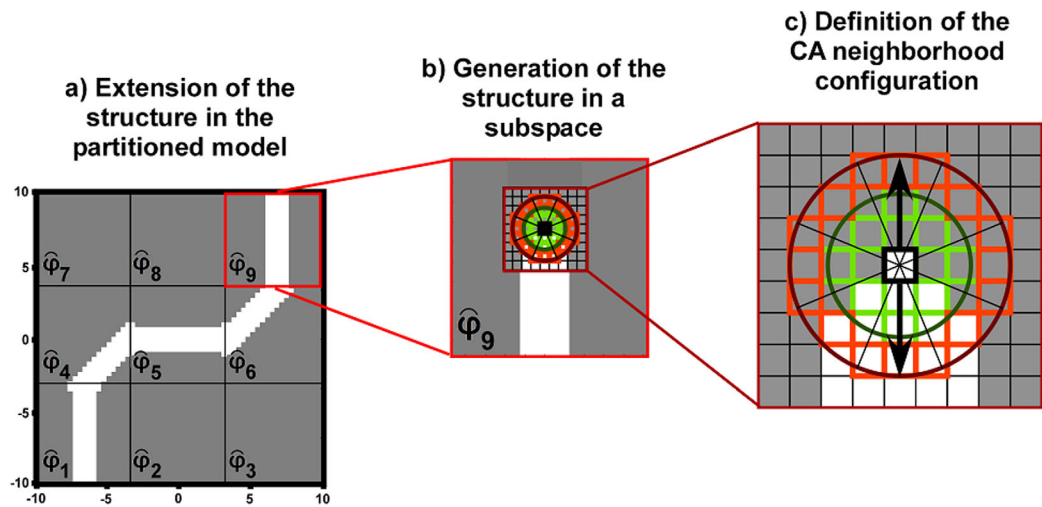


**Figure 1.** Scheme explaining how the CA are used in the CADI model. In the figure gray occurs for state “background” and white for state “structure.” The model is partitioned in  $m_{CA}$  independent CA subspaces (here  $m_{CA} = 9$ ). During the generation process the structure will go through different CA subspaces (a) and will be generated in the local direction assigned by the structural parameters piloting these CA (b). Along the generation direction the CA will modify the property values of the model cells it controls (represented by the squares lattice in Figure 1c).

The CA is a discrete time-evolving system in which a cell of the system is defined by its state and its neighborhood. At a CA time step  $t_{CA} + 1$ , the state of each cell will simultaneously evolve to a new one depending on a constant transition rule involving the state of a cell and the states of the cells in its neighborhood at the time step  $t_{CA}$ . Thus, a CA subspace of the model proposed in the CADI algorithm can be described as a quadruple  $\langle \varphi, Z, N, T \rangle$  [Sun et al., 2011; Van der Weeën et al., 2011]:

1.  $\varphi$  is a subspace of the global model, discretized as a lattice of  $c$  cells.
2.  $Z$  is a function returning the states values for each selected cells of the subspace at a specified time step (with two possible states:  $Z_{t_{CA}}(c_i) = \beta_{background}$  or  $Z_{t_{CA}}(c_i) = \beta_{structure}$ , where  $\beta_{background}$  and  $\beta_{structure}$  are the parameterized values assigned to the properties of the structure and the background in the subspace).
3.  $N$  is a neighborhood function that selects among all cells of the subspace the subset of cells that are considered in the neighborhood of a given cell  $c_i$ .
4.  $T$  is a function of cell-state transition rule. Thus, a transition in the CA for a given cell  $c_i$  is expressed as  $Z_{t_{CA}+1}(c_i) = T(Z_{t_{CA}}(N(c_i)))$ , and a full transition in the CA process (considering all cells of the subspace lattice) is  $\varphi_{t_{CA}+1} = Z_{t_{CA}+1}(c_i), \forall i$ .

The choice of  $N$  and  $T$  for the CA in this work will be detailed in the following paragraphs. The CA will be used to produce a spatial linear structure in the model. The global model is partitioned in several subspaces, each one being discretized as a lattice of  $c$  squared cells (Figure 1c). Each cell of a subspace  $\varphi$  can be in only two possible different states: state “background” which take a value  $\beta_{background}$ , or state “structure” which take a value  $\beta_{structure}$ . So, a subspace has a binary distribution.  $\beta_{structure}$  is homogeneous within a subspace but can vary among the different subspaces.

Commonly, CA use neighborhood sequencing such as the Moore or the Von Neumann neighborhood rules (see Appendix 1) [Moore, 1962; Von Neumann and Burks, 1966]. But here we chose  $N$  as a dual-radius neighborhood definition as presented in Figure 2. Two circles of cells, defined by their cell-radius  $R_{inner}$  and  $R_{outer}$ , are centered on a given cell  $c_i$  (for a full CA time step transition  $c_i$  would be alternatively each cell of the CA subspace). The inner circle defines the “activator” cells for  $c_i$  (green in Figure 2) and the outer circle defines the “inhibitor” cells for  $c_i$  (orange in Figure 2). The terms “activators” and “inhibitors” are relative only to the cells in “background” state: the cells in state “background” in the “activator” neighborhood will tend to transform the cell  $c_i$  in a state “background” while the cells in state “background” in the “inhibitor” neighborhood will tend to transform the cell  $c_i$  in a state “structure.” The balance of the ratio of “background” cells in each “activator” and “inhibitor” neighborhoods can be disturbed by the existence of cells in state “structure” (for example the presence of a cell in state “structure” in the “activator” neighborhood of a cell  $c_i$

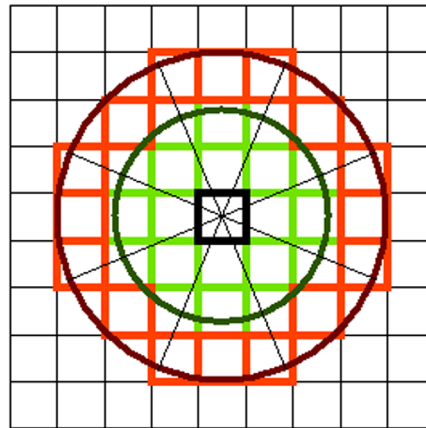


**Figure 2.** An example of the dual-radius neighborhood considered in our CA definition. The black highlighted cell is the cell under consideration in this example (each cell of the lattice would alternatively be considered during a full CA time step). The green highlighted cells are considered as its “activators” neighbors in the transition rule and the orange highlighted cells as its “inhibitors” neighbors. These cells are selected by an inner and an outer circle (in bold) with configurable radius which permit the configuration of the neighborhood. In this example, the inner circle has a radius = 2 and the outer circle has a radius = 3. Additionally, the neighborhood is split into 2 × 8 sectors (by the radial lines) which permit a more configurable weighting definition (see Figure 4).

will reduce the amount of cells in state “background” in this “activator” neighborhood compared to in the “inhibitor” neighborhood, and thus the cell  $c_i$  would then become “structure”. The cells outside of the circles are not considered for the state transition of the cell  $c_i$ . This definition can be seen as an extension of the Von Neumann rules, by adding inhibitors neighbors to activators cells that follow a Von Neumann neighborhood. Additionally, each circle of the neighborhood definition was radially split into eight sectors to allow for spatially variable weighting of activators and inhibitors cells, in order to privilege particular directions during the generation (see Figure 4).

During the transition to  $t_{CA}+1$ , the transition rule  $T$  defines alternatively for each cell of the lattice the new state of a cell  $c_i$  by considering the equilibrium of activators and inhibitors cells in state background ( $\beta_{background}$ ) in its neighborhood  $N(c_i)$  at the instant  $t_{CA}$ . Therefore, the neighborhood configuration associates cells values in the activator zone to a positive weighting (+) and cells values in the inhibitor zone to a negative weighting (−). The weighted values in each of eight activator and inhibitor sectors are then also corrected by an additional balancing weight (ratio between the number of cells in a sector and the total number of cells), in order to have the same consideration between each sector of the neighborhood. In fact, each sector does not contain the same amount of cells, due to the consideration of deformations of circles in a lattice of squares. Finally, the transition rule  $T$  sums the weighted val-

ues from all cells in state  $\beta_{background}$  in the neighborhood  $N(c_i)$ . If the total weight of activators in state  $\beta_{background}$  is higher (the sum is positive), the cell  $c_i$  will take the value  $\beta_{background}$  (“background”), if the total weight of inhibitor in state  $\beta_{background}$  is higher (the sum is negative), the cell  $c_i$  will take the value  $\beta_{structure}$  (“structure”)

$$T(c_i) = \sum_{k=1}^{ncell} Z_{t_{CA}}^{weight}(c_k) \text{ for } c_k \in [N(c_i)] \cap [Z_{t_{CA}}(c_k) = \beta_{background}] \tag{1}$$

$$Z_{t_{CA}+1}(c_i) = \beta_{background} \text{ if } T(c_i) \geq 0, \quad Z_{t_{CA}+1}(c_i) = \beta_{structure} \text{ if } T(c_i) < 0,$$

where  $ncell$  denotes the total number of cells in  $N(c_i)$  and  $Z_{t_{CA}}^{weight}$  is the function returning the state value taking into account the weighting parameterization from the neighborhood.

After sufficient time steps of the CA with the same transition rule, the subspace  $\varphi$  will converge to a stable geometry  $\hat{\varphi}$  (the geometry will not change over increasing CA time steps anymore) depending on the weighting parameterization given to the neighborhood definition  $N$  (Figure 3).

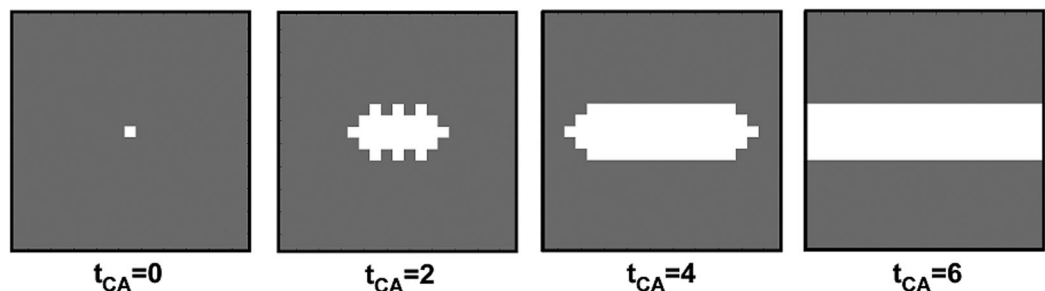


**Figure 3.** Time evolution of a CA configured with a neighborhood weighting defining a horizontal structure generation (see Figure 4). After the sixth time step the CA has converged and its geometry is stable over the following steps. Here gray occurs for state “background” and white for state “structure.”

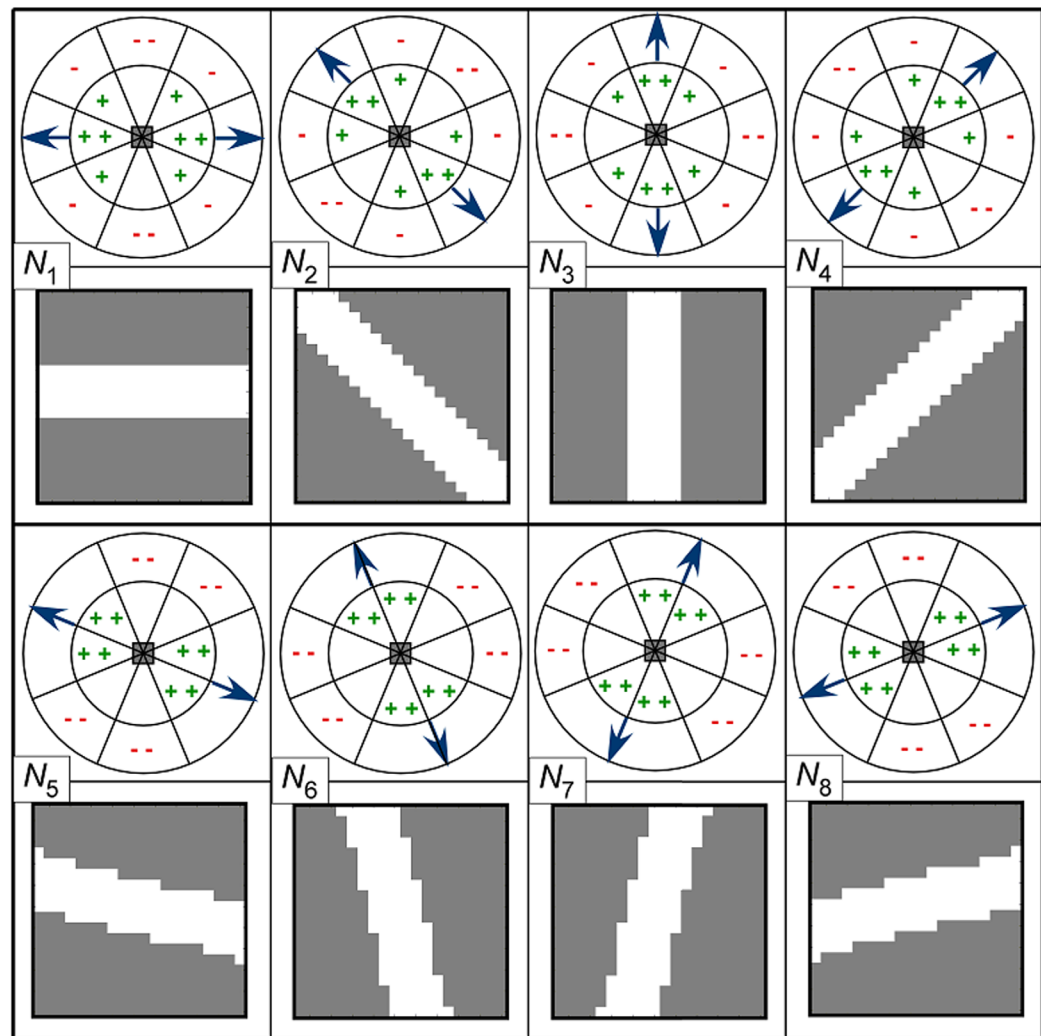


**Figure 4.** Presentation of eight different stable structures started by a unique centered cell, and their associated CA neighborhood configuration. The grayed cell in the neighborhood configuration is a given cell considered during the CA process. It is surrounded by its neighbor cells, which are not shown for reasons of readability. Its neighborhood is split in eight internal “activator” sectors and eight external “inhibitor” sectors, each one being assigned to a given weight. A “++” occurs for a positive weight for the neighbor cells in the area, a “+” weight is twice higher than a positive weight represented by a single “+.” A “--” occurs for a negative weight for the neighbor cells in the area, a “-” weight is twice higher than a negative weight represented by a single “-.” An empty part of the neighborhood occurs for a null weight, meaning that cells in the area are not considered in the transition rule. Here we present the CA configuration leading to eight different structure directions which will be considered as suborientation of the global structure in the model. In the structural map, gray occurs for state “background” and white for state “structure.”

Thus, playing on the weighting distribution in the divided activator and inhibitor sectors, and on the radius  $R_{inner}$  and  $R_{outer}$  of the neighborhood definition  $N$ , the CA can produce linear structures in eight directions from a unique starting cell, as shown in Figure 4. The weighting distribution defining each direction has been empirically specified.

On the presented configurations, the starting cell is considered in the center of the lattice. The neighborhood weighting permits to modify the direction of the structure and the radius values modify its aperture. These eight weighted neighborhood configuration functions  $N_i, i \in [1, 8]$  will be considered as the different configuration possibilities in the subspaces parameterization in the dynamic structural optimization process of the inversion algorithm (presented in the section 3.1). Thus, in the CADI algorithm a CA subspace of the model is parameterized by two parameters: its structural direction (neighborhood configuration  $N$ ) among the eight possible and its values of property  $\beta = [\beta_{background}, \beta_{structure}]$ . Therefore, a converged configuration of a parameterized subspace will be expressed as  $\hat{\varphi}(N, \beta)$  (using one of the eight different direction configuration  $N_i$ , as presented in Figure 4).

The geometry of a structure over the entire model  $\Gamma$  (composed of all converged subspaces  $\hat{\varphi}_k(N, \beta), k \in [1, m_{CA}]$ ) can be defined in the CA generation process with only two “pilot” vectors containing each subspaces parameters. This piloted model can be expressed as  $\Gamma(P_N, P_\beta)$ , where  $P_N$  is a  $m_{CA}$  vector containing the direction of generation (configured by the weighted neighborhood configurations  $N_i, i \in [1, 8]$ ) assigned to each CA subspace of the model, and  $P_\beta$  a  $m_{CA} + 1$  vector containing the  $\beta_{structure}$  values assigned to the “structure” cells in each of the  $m_{CA}$  CA subspaces and also the  $\beta_{background}$  value (the background being considered, in this paper, as uniform, but it could also be possible to consider a  $\beta_{background}$  value for each subspace). Thus, by piloting the CA generation process with only  $P_N$  and  $P_\beta$  as parameters we can generate the whole model as shown in Figure 1. The aperture all along the structure is considered as constant and can be configured with the CA neighborhood radius values and the partitioning of the model.

The CA generation process of the structure starts from an entire “background” ( $\beta_{background}$ ) state model with only one or several selected cell(s) of the model in state structure ( $\beta_{structure}$ ) which are considered as the starting point(s) of the structure. At the firsts CA time steps, the structure will be generated only in the subspaces where initial structure cells are defined. Each boundary cells state at the edge of a CA subspace is symmetrically transferred to the boundary cells of the adjacent CA. Therefore when the structure arrives to the limit of its first subspace, it can enter a new CA subspace by local symmetry at the boundary limit between them. The new CA subspace the structure has entered has potentially another neighborhood definition; thus, the structure will follow a new direction from there. Once the structure has been generated in a subspace, this subspace becomes “inhibited” to another generation (the structure can enter only one time each subspace). And so the structure will propagate within the model, through the increasing CA time steps, until it reaches a stable geometry  $\Gamma(P_N, P_\beta)$  (see Figure 1).

### 2.2. Statement of Inverse Problem

The inverse problem involves a formulation of the forward problem which links the spatial properties of the model to the data

$$d = f(\Gamma(P_N, P_\beta)) + \varepsilon, \tag{2}$$

where  $\Gamma(P_N, P_\beta)$  is the spatial distribution of the  $m$  properties cells in the model. The cells of the model take their values from a finite set  $P_\beta$  and are structured by the CA directions  $P_N$ ,  $d$  is a vector of  $n$  modeled data,  $f$  is a forward problem application  $\mathbb{R}^m \rightarrow \mathbb{R}^n$ , and  $\varepsilon$  represents the observed data error.

In a probabilistic framework, the aim of the inverse problem is to find the most probable models considering  $P_N$  and  $P_\beta$  as parameters constrained by the observed data and the prior information on both parameters. This inverse issue can be treated as a sequential inversion. First, for a given  $P_\beta$ , we determine the geometry of the structure via the estimation of  $P_N$ , which is then used in the second time to infer the values of  $P_\beta$ . Using a Bayesian approach on Gaussian probability density functions, the problem can be formulated by two posterior probability densities  $\rho_{structure}(P_N|d, P_\beta)$  and  $\rho_{properties}(P_\beta|d, P_N)$  in order to image the geometry of structure controlled by  $P_N$  and their physical property values controlled by  $P_\beta$

$$\begin{aligned} \rho_{structure}(P_N|d_{obs}, P_\beta) &\propto \rho(d_{obs}|P_N, P_\beta) \cdot \rho(P_N) \\ &\propto \exp\left(-\frac{1}{2}(d_{obs} - f(\Gamma(P_N, P_\beta)))^T C_d^{-1} (d_{obs} - f(\Gamma(P_N, P_\beta)))\right), \\ &\times \exp\left(-\frac{1}{2}(P_{N,prior} - P_N)^T C_{P_N}^{-1} (P_{N,prior} - P_N)\right) \end{aligned} \tag{3}$$

$$\begin{aligned} \rho_{properties}(P_\beta|d_{obs}, P_N) &\propto \rho(d_{obs}|P_\beta, P_N) \cdot \rho(P_\beta) \\ &\propto \exp\left(-\frac{1}{2}(d_{obs} - f(\Gamma(P_N, P_\beta)))^T C_d^{-1} (d_{obs} - f(\Gamma(P_N, P_\beta)))\right), \\ &\times \exp\left(-\frac{1}{2}(P_{\beta,prior} - P_\beta)^T C_{P_\beta}^{-1} (P_{\beta,prior} - P_\beta)\right) \end{aligned} \tag{4}$$

with  $\rho$  denotes the Gaussian probability density function.  $\rho(d_{obs}|P_N, P_\beta)$  is the likelihood function;  $\rho(P_N)$  and  $\rho(P_\beta)$  represent a priori information on the parameters  $P_N$  and  $P_\beta$ .  $d_{obs}$  is the  $(1 \times n)$  vector of observed data.  $P_{\beta,prior}$  and  $P_{N,prior}$  are the prior models (parameter assumptions) on the unknown parameters  $P_\beta$  and

$P_N$ , chosen by the modeler to constrain the inversion.  $C_d$  ( $n \times n$ ),  $C_{P_N}$  ( $m_{CA} \times m_{CA}$ ), and  $C_{P_\beta}$  ( $(m_{CA} + 1) \times (m_{CA} + 1)$ ) are covariance matrices of the expected uncertainties on data and the prior models.  $C_{P_N}$  and  $C_{P_\beta}$  can also be seen as weighting values in the objective function to constrain the inversion result to have subspaces property values and directions remaining close to the parameters chosen in the prior models. The maximization of the posterior probability densities (equations (3) and (4)) can be achieved by a minimization of the following objective functions in the inversion process [Tarantola and Valette, 1982]:

$$\Psi_{structure}(P_N) = \frac{1}{2} (d_{obs} - f(\Gamma(P_N, P_\beta)))^T C_d^{-1} (d_{obs} - f(\Gamma(P_N, P_\beta))) + \frac{1}{2} (P_{N,prior} - P_N)^T C_{P_N}^{-1} (P_{N,prior} - P_N), \tag{5}$$

$$\Psi_{properties}(P_\beta) = \frac{1}{2} (d_{obs} - f(\Gamma(P_N, P_\beta)))^T C_d^{-1} (d_{obs} - f(\Gamma(P_N, P_\beta))) + \frac{1}{2} (P_{\beta,prior} - P_\beta)^T C_{P_\beta}^{-1} (P_{\beta,prior} - P_\beta). \tag{6}$$

This minimization can be achieved iteratively with sequential optimizations on the geometry of the structure and on the values taken by the properties. The convergence of these two objective functions to their minimal values depends on the parameterization of the model and its initialization. A global minimization is not guaranteed, as the result of the inversion depends of the initial model. However, the optimum can be explored by leading several inversions starting from different initial models. The different steps of the CADI algorithm are presented in Figure 5. The structural and property values parameters in  $P_N$  and  $P_\beta$  are first initialized to generate the initial model. This initialization consists in assigning an initial reasonable direction of generation and initial property values  $\beta_{structure}$  and  $\beta_{background}$  to each CA subspaces in the model. After this initialization part, a sequential inversion process will first conduct an iterative structural optimization in which the CA structural generation process will regenerate the model with the updated parameters at each iteration. Once this optimization is completed, the inversion will continue with an optimization of the property values for the previously inverted structure. The process is then ended by an estimation of uncertainties on the structure geometry and on the property values. These different parts of the inversion process are detailed in the following sections.

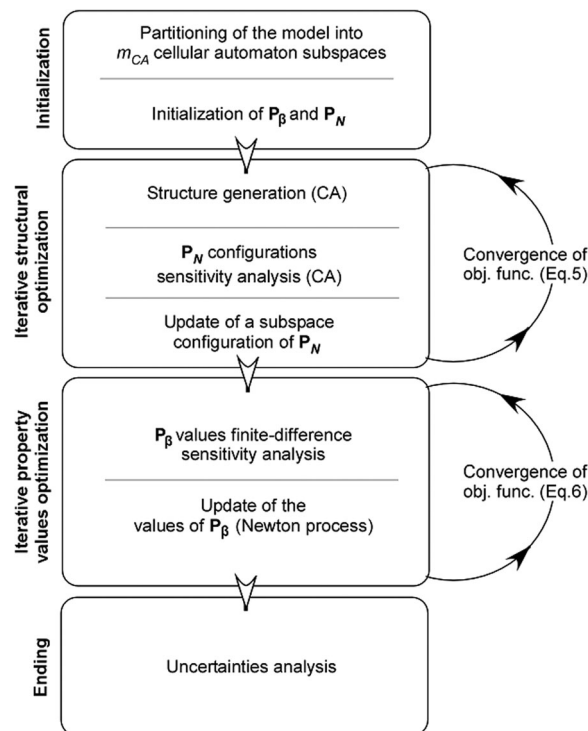


**Figure 5.** Operating scheme for the Cellular Automata-based Deterministic Inversion (CADI) algorithm. After an initialization of  $P_N$  and  $P_\beta$  with chosen directions and property values for each subspace, the algorithm begins an iterative process. It will first optimize the geometry of the structure in the model by iteratively updating the structural model using the CA generation process. Once the objective function has converged to a local minimum on the structure, it will lead a second optimization on the values of the properties for the previously inverted structure, until the objective function converges to a local minimum again. Finally, the uncertainties on the structure and the properties of the model are estimated.

After this initialization part, a sequential inversion process will first conduct an iterative structural optimization in which the CA structural generation process will regenerate the model with the updated parameters at each iteration. Once this optimization is completed, the inversion will continue with an optimization of the property values for the previously inverted structure. The process is then ended by an estimation of uncertainties on the structure geometry and on the property values. These different parts of the inversion process are detailed in the following sections.

### 3. Optimization Process

#### 3.1. Structural Optimization

Initially, a chosen set of probable property values  $P_{\beta,ini}$  and chosen direction configurations  $P_{N,ini}$  are assigned to the piloted model to build an initial model. The aim of the structural optimization will be to modify iteratively the structure piloted by  $P_N$  for a given distribution of  $P_\beta$  until the convergence of the objective function (equation (5)). The modification of the configuration  $P_N$  is defined through a sensitivity analysis.

At an iteration step  $k$ , the sensitivity on the structure is estimated by introducing “perturbations” in the generation and by analyzing the responses by solving the forward problem. Here a perturbation consists in a modification of the configuration  $N$  in a CA subspace of the model (i.e., a local direction modification), the other subspaces configurations remaining unchanged. The structural inversion sensitivity analysis tests the eight configuration possibilities  $N_i, i \in [1, 8]$  as parameter in each CA subspace in order to optimize the geometry of the structure regarding the objective function. This sensitivity analysis is led on the entire model to create a  $8 \times m_{CA}$  sensitivity matrix  $S$ . Thus, at the  $k$ th iteration and for a perturbation using a configuration  $N_i$  in a subspace  $j$ , the element  $(i,j)$  of the sensitivity matrix is defined as

$$S^k(i, j) = \frac{1}{2} \left( d_{obs} - f \left( \Gamma \left( P_N^k |_{P_N^k(j)=N_i}, P_\beta \right) \right) \right)^T C_d^{-1} \left( d_{obs} - f \left( \Gamma \left( P_N^k |_{P_N^k(j)=N_i}, P_\beta \right) \right) \right) + \frac{1}{2} (P_{N,prior}(j) - N_i)^T C_{P_N}^{-1} (P_{N,prior}(j) - N_i), \tag{7}$$

where  $f \left( \Gamma \left( P_N^k |_{P_N^k(j)=N_i}, P_\beta \right) \right)$  represents the modeled data through this perturbation for a given model of  $P_\beta$ , and  $P_{N,prior}(j) - N_i$  represents the angular gap between the prior subdirection and the perturbation direction. Here the sensitivity analysis does not involve variations in  $P_\beta$ , it determines all possible variations of the objective function for a single modification in the structure geometry.

The best improvement is found with the index  $(i, j)_{min}$  in matrix  $S$ , representing the minimal value in the matrix which will give the best improvement for the minimization of the objective function ( $i$  gives the updated configuration  $N_i$  for the CA in the subspace  $j$  of the model). Thus, from a structural parameter set  $P_N^k$ , the optimized set  $P_N^{k+1}$  is built as  $P_N^{k+1} = P_N^k$  except for its index  $j$ :  $P_N^{k+1}(j) = N_i$ . By updating the subspace which gives the best structural improvement, a new structure will be generated for the iteration  $k + 1$ . The algorithm reproduces the same sensitivity analysis for each iteration until the convergence of the objective function. The total number of forward problems evaluations for a structural iteration is  $8 \times m_{CA} + 1$  (with  $8 \times m_{CA}$  evaluations for the sensitivity analysis and 1 for the updated objective function calculation).

At the end of the inversion process, the uncertainties on the inverted structure are estimated through an uncertainties analysis on each subspace of the structure. Due to difficulty to infer the posterior covariance matrix of the structural inversion, this analysis is done for each subspace by inverting the difference between the posterior objective function and the sum of sensitivity values for all CA configuration possibilities, and the prior uncertainties for the subspace  $j$

$$S^{post}(j) = \left( \frac{1}{8} \sum_{i=1}^8 S(i, j) - \Psi_{structure}^{post} + C_{P_N}^{-1}(j, j) \right)^{-1}, \tag{8}$$

with  $S^{post}(j)$  is the posterior structural uncertainty for a subspace  $j$  in the model,  $i$  denotes the different rows of the matrix  $S$  of the last iteration, and  $\Psi_{structure}^{post}$  is the value of the minimized objective function after convergence.

If a subspace is well-constrained, its value  $S^{post}$  should be low (another structure direction would have a negative impact in the minimization of the objective function), and if not, this value should be high (another structure direction would be quite neutral in the minimization of the objective function).

### 3.2. Property Values Optimization

Once the structure is optimized, the property parameters  $P_\beta$  taken by the CA subspaces of the model are then also iteratively optimized, for the inverted structure; using a finite difference approach for the sensitivity analysis (for  $m_{CA} + 1$  unknown property values to optimize, including  $m_{CA}$   $\beta_{structure}$  values plus one common value for  $\beta_{background}$ ). The Jacobian sensitivity matrix  $J(n \times (m_{CA} + 1))$ , for an index  $(i, j)$  is defined as

$$J(i, j) = \left. \frac{\partial f_i}{\partial P_\beta} \right|_{P_\beta(j) = P_\beta(j) + \Delta P_\beta}, \tag{9}$$

with  $f_i$  the forward problem on a data  $i$  for a variation  $\Delta P_\beta$  of  $P_\beta(j)$ . Here  $\Delta P_\beta$  is the finite difference step.

The new values  $P_\beta^{k+1}$  from a previous set  $P_\beta^k$  are calculated from a linearization of (equation (6))

$$f(\mathbf{P}_\beta^{k+1}) \approx f(\mathbf{P}_\beta^k) + \mathbf{J}^k \cdot (\mathbf{P}_\beta^{k+1} - \mathbf{P}_\beta^k). \tag{10}$$

The optimization of  $\mathbf{P}_\beta$  is achieved via a Newton iterative process, initialized at a reasonable  $\mathbf{P}_{\beta,ini}$  [Tarantola and Valette, 1982]. For the  $k + 1$ th step in the iterative process

$$\mathbf{P}_\beta^{k+1} = \mathbf{P}_\beta^k + \left( (\mathbf{J}^k)^T \cdot \mathbf{C}_d^{-1} \cdot \mathbf{J}^k + \mathbf{C}_{\mathbf{P}_\beta}^{-1} \right)^{-1} \cdot (\mathbf{J}^k)^T \cdot \mathbf{C}_d^{-1} \cdot (\mathbf{d}_{obs} - f(\Gamma(\mathbf{P}_N, \mathbf{P}_\beta^k))) + \mathbf{C}_{\mathbf{P}_\beta}^{-1} \cdot (\mathbf{P}_{\beta,prior} - \mathbf{P}_\beta^k). \tag{11}$$

The total number of forward problems in an iteration for the property value sensitivity evaluation in a model with a uniform background will be  $m_{CA} + 1$ , while for a model with a varying background among the CA subspaces it would require  $2 \times m_{CA}$  evaluations. Then the compute of the updated objective function requires one more forward problem evaluation.

The uncertainties on the values of properties, calculated at the end of the inversion process, are given by the diagonal entries of the posterior covariance matrix

$$\mathbf{C}_{\mathbf{P}_\beta}^{post} = \left( (\mathbf{J}^{post})^T \cdot \mathbf{C}_d^{-1} \cdot \mathbf{J}^{post} + \mathbf{C}_{\mathbf{P}_\beta}^{-1} \right)^{-1}. \tag{12}$$

These values represent variances of the properties. Then, the square root of the diagonal entries represent their standard deviation.

#### 4. Applications

The CADI algorithm has been tested on six theoretical study cases for a linear inversion of a simple structure (Study case 1), a more complex structure (Study case 2), a complex multidirectional structure (Study case 3) and for a linear, nonlinear and joint inversions (Study cases 4–6) of a geostatistical generated structure. For these different examples we did not use any prior information on the structure in  $\mathbf{P}_{N,prior}$  but we incorporated constant measurement errors in a diagonal matrix  $\mathbf{C}_d = \sigma_{data}^2 \cdot \text{Id}(n)$ , and prior background and structure property values in  $\mathbf{P}_{\beta,prior}$  with their covariances in a diagonal matrix  $\mathbf{C}_{\mathbf{P}_\beta} = \sigma_\beta^2 \cdot \text{Id}(m_{CA} + 1)$ . These six study cases and their results are presented in Table 1, and the theoretical true structures to be reproduced are presented in Figure 6.

##### 4.1. Study Case 1

The first study case is a linear inversion of a simple structure. The purpose of this study case is essentially to illustrate how the optimization within the CA subspaces in the structural inversion works. For the linear inversion, we considered seismic data. The properties taken into account in the model are the seismic

**Table 1.** Inversion Results Obtained for the Six Different Study Cases<sup>a</sup>

	Inversion Type	Number of Cells (m)	Number of Data	Number of Iteration	Data R <sup>2</sup>	Structural Similarity	Inversion Time
		CA Grid	Error Variance				
Case 1 (Figure 5a)	Linear	3,600 (3 × 3)	358 $\sigma_{data}^2 = 1$ ms	4	0.99	99.7%	4 min
Case 2 (Figure 5b)	Linear	10,000 (5 × 5)	598 $\sigma_{data}^2 = 1$ ms	21	0.96	97.9%	1.3 h
Case 3 (Figure 5c)	Linear	48,400 (11 × 11)	1,318 $\sigma_{data}^2 = 1$ ms	Nolnit: 26 Init: 30	0.91 0.96	97.1% 98.3%	13.2 h 18.8 h
Case 4 (Figure 5d)	Nonlinear	3,600 (3 × 3)	128 $\sigma_{data}^2 = 0.1$ m	7	0.98	85.8%	13 min
Case 5 (Figure 5d)	Linear	3,600 (3 × 3)	358 $\sigma_{data}^2 = 1$ ms	4	0.99	82.6%	4 min
Case 6 (Figure 5d)	Joint: Linear + nonlinear	3,600 (3 × 3)	486 $\sigma_{data}^2 = 1$ ms, $\sigma_{data}^2 = 0.1$ m	7	NL = 0.98 L = 0.99	88.2%	20 min

<sup>a</sup>This table includes the inversion type, the number of cells of the model, the partitioning and the observed data considered in the inverse modeling, the error variance of data, the number of iteration necessary to the convergence of the inversion process, the proximity between inverted data and observed data (R<sup>2</sup>) and between the inverted structure and the true one pixel wise (structural similarity), and the inversion time. In case 3, Nolnit = initial simple model and Init = initial more complex model. In case 6, NL = nonlinear and L = linear.

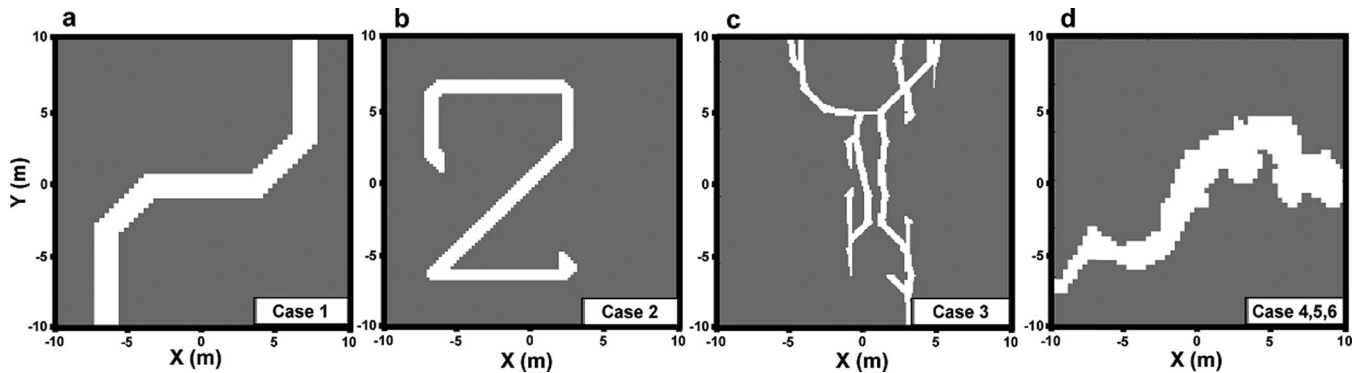


**Figure 6.** Presentation of the four different structures tested in the six study cases in this paper. (a) The case 1 is a linear inversion of a simple geometry to show how the optimization works. (b) The case 2 is a linear inversion of a more complex geometry. (c) The case 3 is a linear inversion of a complex multidirectional linear structure. (d) The cases 4–6 are linear, nonlinear, and joint inversion of a geostatistical generated geometry, appearing as a more natural structure.

velocities. Our simple synthetic model (Figure 6a) is set up as a field of  $20 \times 20 \text{ m}^2$  with a perfectly uniform matrix (background) with a seismic velocity of 3.33 km/s, and an empty conduit (structure) of 0.26 km/s. The model properties are discretized in a  $60 \times 60$  regular grid. Seismic transmitters and receptors are set up around the theoretical model, at the beginning and end of each row, column and diagonal of the model grid, which would correspond to a device every 33 cm. The observed data consists on travel time from seismic waves traveling through the model. The seismic wave travel time is calculated by summing the products between inverse of seismic velocity and distance traveled in each cell swept by the wave following the shortest path in the grid (in this case by summing cells in rows, columns and diagonals). If each cell of the grid swept divides the path followed by the wave, the total travel time of the wave is

$$t_{wave} = \sum_{i=1}^{\eta} \frac{1}{s_i} \cdot \Delta x_i, \quad (13)$$

where  $t_{wave}$  design the travel time of the wave (in ms),  $i \in [1, \eta]$  identifies the different  $\eta$  cells swept by the wave during its travel,  $s_i$  is their seismic velocities (m/ms or km/s), and  $\Delta x_i$  the distance traveled by the wave through these cells (m).

Thereby, 358 observed data were generated from the theoretical model and will be used for the inversion process. For this simple geometry structure, the inversion algorithm was conducted using a relatively coarse  $3 \times 3$  CA partitioning, and by considering a simple straight structure initially (Figure 7a) with seismic velocities of 2 km/s for the background and 0.5 km/s in the structure. The covariance matrix  $C_{\beta}$  was generated with a seismic velocity variance of  $\sigma_{\beta}^2 = 1 \text{ km/s}$  and the seismic velocities of the initial model were also taken as prior values in  $P_{\beta, \text{prior}}$ . The inversion converged in four iterations.

This case permits to understand how the CADI algorithm works. Each different step of the optimization of the model is presented in Figure 7. Starting from the initial structure in Figure 7a, for each next steps the optimization process tries to find new subdirections improving the initial structure over the partitioning of the model (shown as a black grid in Figure 7). At the first step (Figure 7b) the initial model was improved in its central part, and at the two next steps (Figures 7c and 7d) the angles of the lower left and upper right parts of the true model were found. The last step of the inversion in Figure 7e corresponds to the properties optimization in order to improve the objective function and find the true properties. With this parameterization of the inverse problem, the result for this study case reproduces the true structure (Figure 8) and the observed data (Table 1) well.

This simple case is useful to show how the CADI algorithm modifies at each step the geometry of the initial structure and thus to understand why the information and the partitioning chosen in the initial model will considerably influence the deterministic process (in term of time but also in term of result as we will see in study case 3).

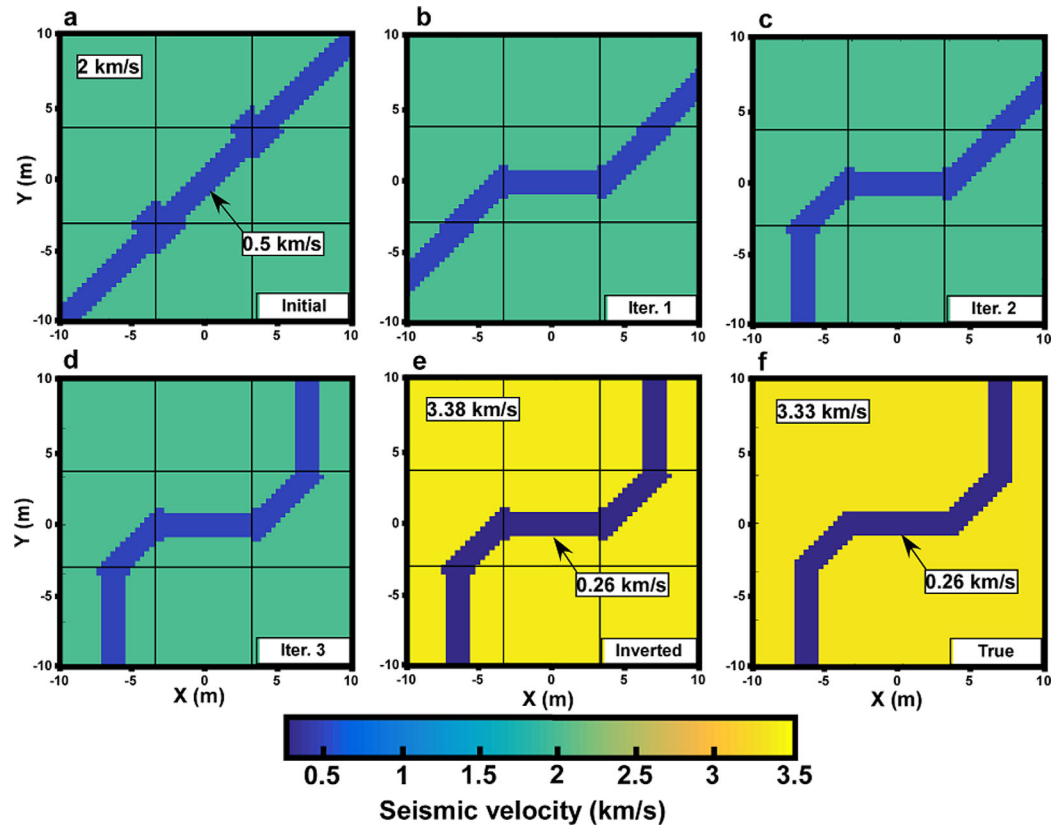


**Figure 7.** Result of the linear inverse modeling of the case study 1. The inversion finished after four iterations. This figure shows all different iterations of the inversion from (a) initial model to (e) inverted model. The true structure is shown in Figure 7f. Figure 7d corresponds to the structural optimization and Figure 7e to the properties optimization for this structure. The different CA subspaces of the model are highlighted by the black lines.

**4.2. Study Case 2**

The CADI algorithm was then applied on a more complex study case to test its capacities to reproduce complex geometries. The theoretical structure under consideration for this case is presented in Figure 6b. As in the first study case, the linear inversion is led by using seismic data, but with other seismic velocities for the matrix (2.5 km/s) and the conduit (0.26 km/s). The model was discretized as a regular grid of 100 × 100 cells. The observed data consist in 598 seismic time travel calculated in the same way than explained for the case study 1. This time, in order to give more possibilities to the structural inverse process, the inverse model was partitioned in a 5 × 5 CA subspaces with the true property values initially known. The covariance matrix  $C_{\beta}$  was generated with a seismic velocity variance of  $\sigma_{\beta}^2 = 1 \text{ km/s}$  and the seismic velocities of the initial model were also taken as prior values in  $P_{\beta, \text{prior}}$ .

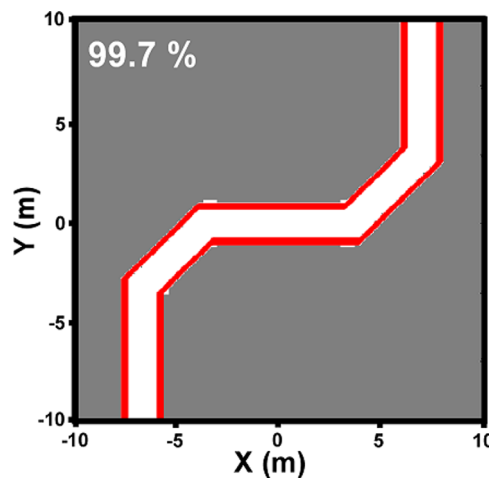


**Figure 8.** Comparison of the optimal structure found by inversion (in white) and the true structure (bold boundaries) for the case study 1. For this simple geometry, the inverse algorithm could easily reproduce the structure.

Initially, we set up a straight linear structure (Figure 9a). The algorithm then converged in 21 iterations (it took approximately 1 h with a computer with 2 processors Intel Xeon 2.4GHz of 16 cores). The Figure 9 shows several steps of the inversion process (Figures 9b–9d), the optimized inverse model in Figure 9e and the true model in Figure 9f.

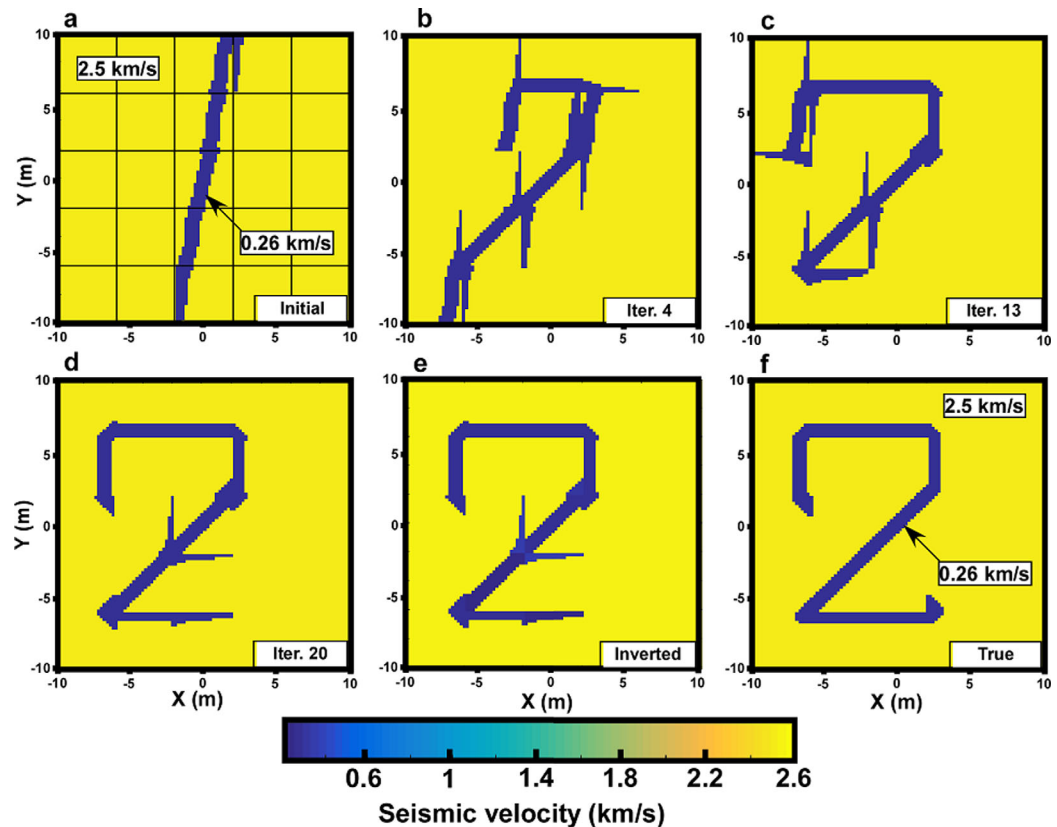


**Figure 9.** Result of the linear inverse modeling of the case study 2. The convergence is performed with 21 iterations. This figure shows some different iterations of the inversion from (a) initial model to (e) inverted model. The true structure is shown in Figure 9f. We noted that the optimization on the property values permits to balance the structural inversion errors. For example, in this case, the structural additions in the center of the model in Figure 9e were optimized by a light augmentation of its seismic velocity (0.5 km/s instead 0.26 km/s).

For this case, the structural inversion is close to the real one but not perfect as in first study case (Figure 10) and we can show in Figure 9e that these imperfections are balanced by the properties optimization. Thus, the zone of the structure with an inverted structural part which does not exist in the true structure (central part) is corrected by a light increase of its seismic velocity in order to minimize the differences between calculated and observed data (0.5 km/s instead of 0.26 km/s). This correction tends to locally slightly approach the structural seismic velocity to the matrix seismic velocity and thus slightly reducing the existence of this local part of the structure in the model. This property values optimization permits a better convergence on the objective function and is, in some cases, useful to counterbalance the approximations of the structural optimization when the property values are initially well known.

### 4.3. Study Case 3

In this third study case we applied the CADI algorithm on a complex multilinear structures network. The study was done to show all the capacities of the CADI method to model fractured fields, which are equivalent to linear structures dispersing in multiple direction among the space. The theoretical structure under consideration for this case is presented in Figure 6c. The linear inversion is led by using seismic data generated with given seismic velocities for the matrix (2.5 km/s) and the conduit (0.33 km/s). The model was discretized as a regular properties grid of  $220 \times 220$  cells. The observed data consist in 1318 seismic time travel calculated in the same way than explained for the case study 1. The inverse model was partitioned in an  $11 \times 11$  CA subspaces with the true property values initially known to investigate the structural optimization capacities.

In this case we compared the sensitivity of the result to the initial model. We set two inversions with two different initial models, the first one being very simple and incorporating only a global direction of

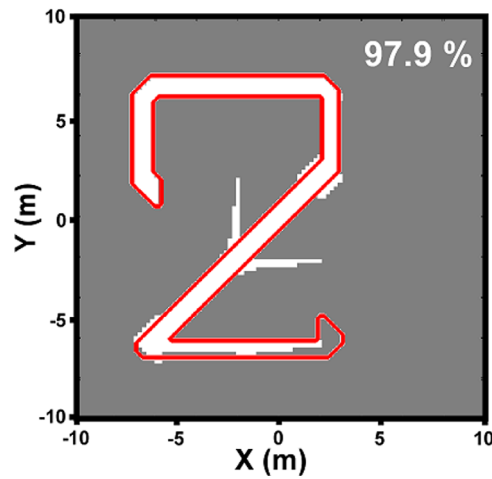


**Figure 10.** Comparison of the optimal structure found by inversion (in white) and the true structure (bold boundaries) for the case study 2. The optimization process reproduced a good structural inversion. The few inversion errors in the center of the model were lightly balanced by the inversion on the properties (see Figure 9).

generation (Figure 11a) and the second one incorporating a bit more information on the structural shape (Figure 11d). Figure 11 shows these initial models, the inverted models they have produced and the comparison between the inverted models and the true one (Figure 6c). For the first inversion the result is already close to the true model, especially considering the simplicity of the initial model. A simple straight structure can become a more complex multidirectional structure through the optimization process and find the main shapes and trends of a complex structure geometry which shows the possibilities given by the parameterization in the CADI algorithm. Starting from a different initial structure in the second inversion we arrived to a slightly better result on the geometry which becomes really close to the true one. It highlights the importance of incorporating some information in the initial model for the inversion process, but however if no information are known, the first inversion shows that even a very simple initial assumption can produce a good result.

**4.4. Study Case 4**

For the fourth study case, a nonlinear inversion has been led on a structure generated by a geostatistical technique using a directionally oriented variogram function with the package gstat in R (Figure 6d), which appears to be more natural than the previous structures. The steady state observed data have been

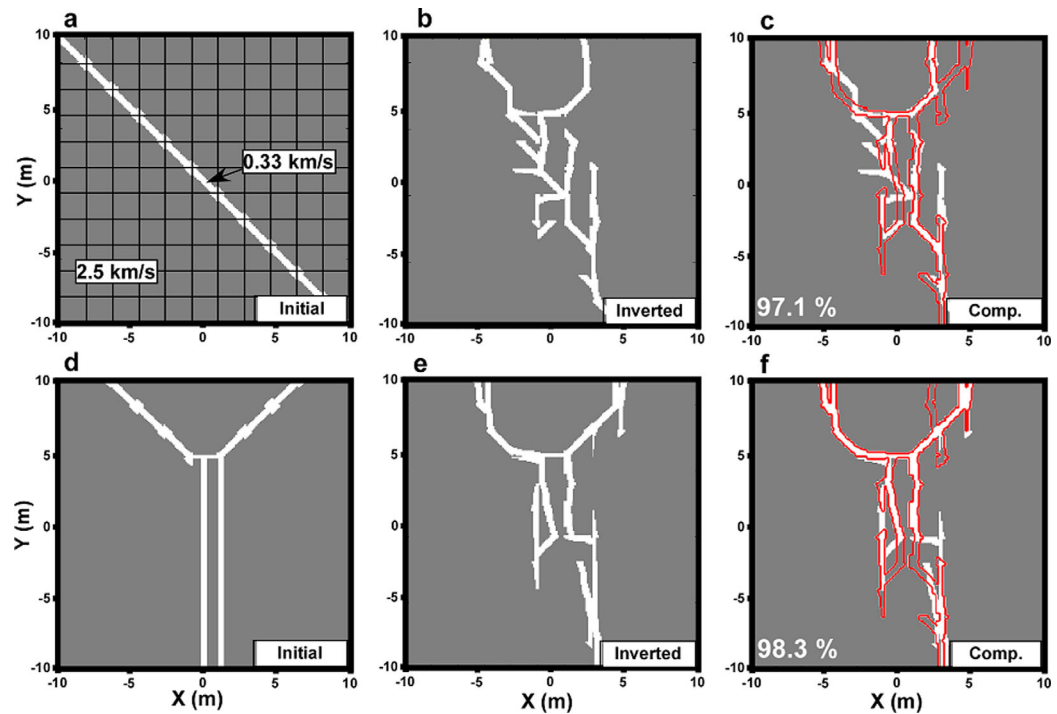


**Figure 11.** Results of the linear inverse modeling of the case study 3. This figure shows two inversions with (a, d) different initial models, (b, e) their results and (c, f) the comparison of these results to the true geometry boundaries in red. The convergence is performed with 26 iterations in the first inversion and 30 iterations in the second. We noted that the information contained in the initial model could slightly modify the result of the inversion but even with a very simple initial case (a) the optimization process permits to find the main shapes and trends of the true structure (c).

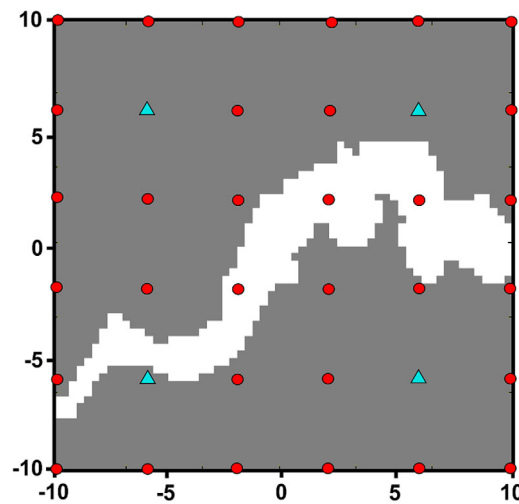


**Figure 12.** Map of the positioning of the wells for the hydraulic tomography inversion for the study case 4. The circles are the position of the measurement piezometers and the triangles are the position of the pumping wells.

produced by a hydraulic tomography with four alternate pumping wells and 32 measurement wells (for a total of 128 observed data) regularly distributed over the model. The positioning of the wells is presented in the model in Figure 12, this model is enclosed in a larger buffer zone ( $1000 \times 1000 \text{ m}^2$ ) defined with a constant head (no drawdown) on its lateral boundary condition and a uniform “background” transmissivity value.

The hydraulic transmissivities are considered as the unknown properties to be inverted in a model with a  $60 \times 60$  cells grid. The theoretical model is set up as a matrix with a transmissivity of  $1.6 \times 10^{-7} \text{ m}^2/\text{s}$  and a structure with an equivalent transmissivity of  $5 \times 10^{-4} \text{ m}^2/\text{s}$ . A  $3 \times 3$  CA partitioning was chosen for the inverse modeling with a good a priori information on the background properties and a structure transmissivity value of  $10^{-3} \text{ m}^2/\text{s}$ . The covariance matrix  $C_\beta$  was generated with a multiplicative variance on the transmissivity of the form

$10^{\pm\sigma_\beta^2}$  where  $\sigma_\beta^2 = 1$  ( $\pm 1$  variance on the transmissivity exponent) and the transmissivities of the initial model were also taken as prior values in  $P_{\beta,prior}$ .

From a straight linear initial structure (Figure 13a), the inversion converged in seven iterations and produced the model presented in Figure 13b. The global trends of the true structure were found although the CADI, as presented previously, produces structures which have a constant aperture. Thus, the inversion process found the best constant-aperture equivalent structure which reproduced the true model for the initial parameters. The properties optimization has permitted to find the true structure property value. However, the initial hydraulic properties did not permit to find the best fitting structure to the true model (Figure 13c). We will show in study case 6 that with the same initial model in a joint inversion, we can have both the true property values and a better fitting structure geometry.

#### 4.5. Study Case 5

A linear inversion has been led on the same geostatistical-generated structure than in study case 4 (Figure 6d). This time, observed data have been produced by seismic, as presented in study case 1 (producing 358

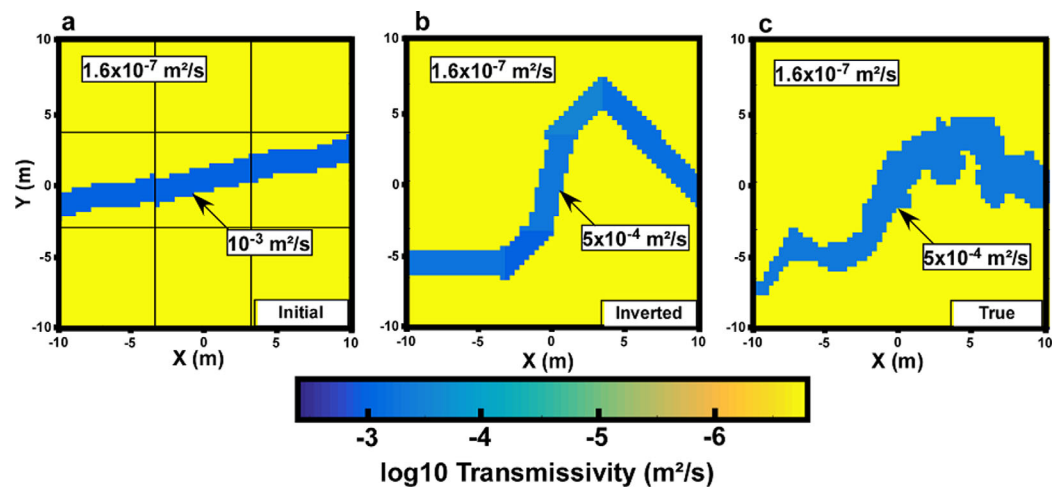


**Figure 13.** Result of the nonlinear inverse modeling of the study case 4. The inversion finished after seven iterations. This figure shows (a) the initial model, (b) the inverted model, and (c) the true structure. The inversion process found an optimized equivalent structure to the initial property value. The true transmissivities were found during the properties optimization.

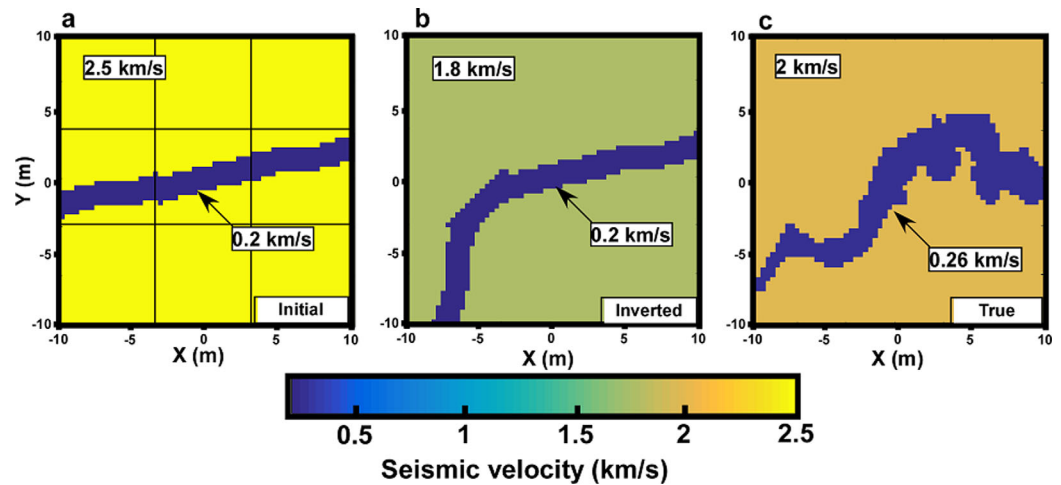


**Figure 14.** Result of the linear inverse modeling of the study case 5. The inversion finished after four iterations. This figure shows (a) the initial model, (b) the inverted model, and (c) the true structure. The structural optimization was limited by the initial properties and by its constant aperture generation to reproduce a variable aperture true structure. In this case, the optimization on the property values permits to balance the initial information and the structural inversion aperture limitations. The properties optimization balanced this limitation by globally decreasing the seismic velocity of the background to a lower value than the true one.

observed data). The seismic velocities are considered as the properties to be inverted in a model with a  $60 \times 60$  cells grid. The theoretical model is set up as a matrix with a seismic velocity of 2 km/s and a structure with a seismic velocity of 0.26 km/s. A  $3 \times 3$  CA partitioning was chosen for the inverse modeling with close initial property values (0.2 km/s for the structure and 2.5 km/s for the background). The covariance matrix  $C_\beta$  was generated with a seismic velocity variance of  $\sigma_\beta^2 = 1$  km/s and the seismic velocities of the initial model were also taken as prior values in  $P_{\beta, \text{prior}}$ .

The inversion converged in four iterations, the results are presented in the Figure 14. With the same initial structure (Figure 14a) than the hydraulic inversion, the seismic inversion produced a slightly different equivalent structure which approximately reproduces global trends of the true structure but is not the best fitting possibility. The properties optimization (Figure 14b) has permitted to balance the structural approximations caused by the limits of the initial information and the generation of a constant-aperture structure. Thus, in the properties optimization, the seismic velocity of the background was decreased under the value of the true one to counterbalance the lower aperture of the generated structure. Thereby, the properties optimization part can bring more flexibility to the algorithm, which is constrained in its structural part by the prior information in the initial condition and its constant aperture. However the inversion process could not truly reproduce the structure and the properties of the true model for the initial parameters. As for the previous nonlinear inversion, we will show in the next study case that a joint inversion permits to reproduce both the property values and a better structure geometry for the same initial parameters.

#### 4.6. Study Case 6

For the last study case, a joint inversion has been led on the same structure generated by a geostatistical approach than in study cases 4 and 5 (Figure 6d). The joint inversion is a simultaneous inversion of different data sets with a same unique inverted structure which has to be able to reproduce the information contained in all different data sets. The information brought by different investigation techniques will reduce the nonuniqueness of the inverse solution, each techniques bringing different information on the parameters [Haber and Oldenburg, 1997]. We have jointly inverted the hydraulic data from study case 4 and the seismic data from study case 5. The joint objective function in this case is a weighted linear combination of the seismic properties objective function and the hydraulic properties objective function. We chose a weighting in order to have initially approximately the same value for each of the two parts of the joint objective function. The observed data were produced by hydraulic tomography and seismic (for a total of 486 observed data). The hydraulic transmissivities and seismic velocities are considered as the properties to be inverted in a model with a  $60 \times 60$  cells grid. The theoretical model is set up with the same property values as presented in study case 4 for the hydraulic properties ( $1.6 \times 10^{-7}$  m<sup>2</sup>/s for the matrix and  $5 \times 10^{-4}$

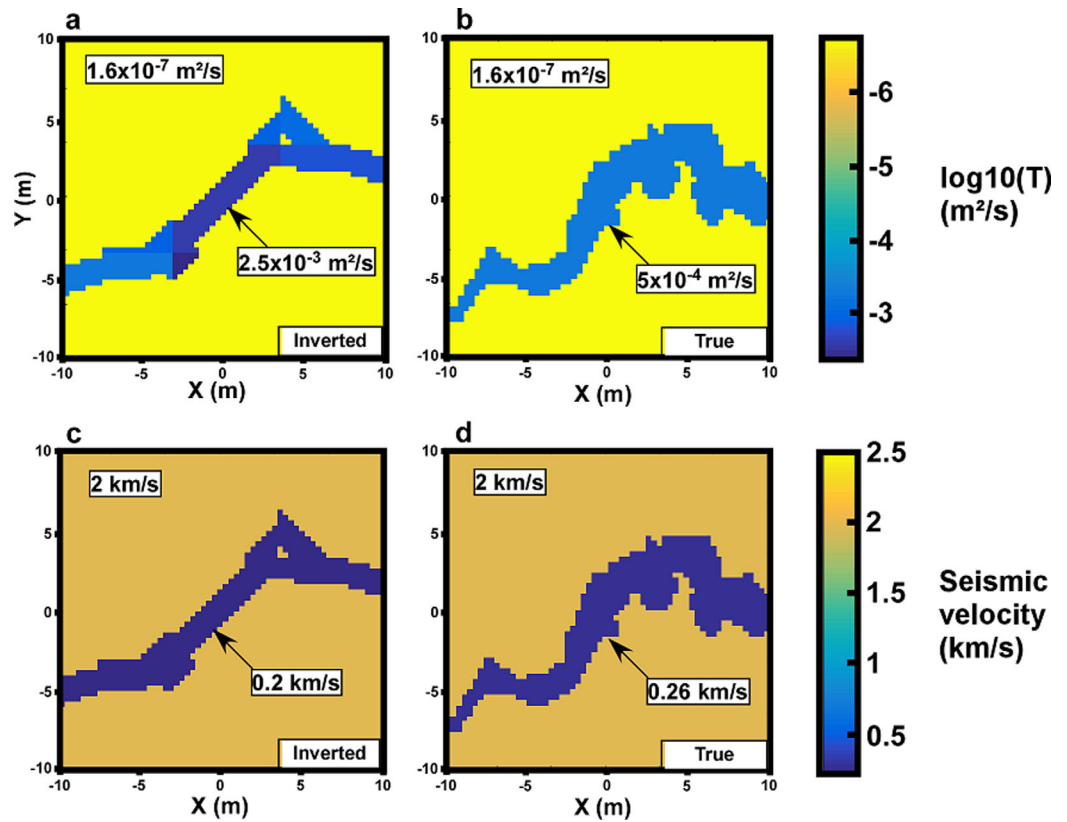


**Figure 15.** Result of the joint inverse modeling of the study case 6. The inversion finished after seven iterations. This figure shows (a) the hydraulic model, (c) the seismic model, and (b, d) the true models. The geometry of the structure in the models was optimized through a joint inversion of seismic and hydraulic data.

m<sup>2</sup>/s for the structure) and in study case 5 for the seismic properties (2 km/s for the matrix and 0.26 km/s for the structure). A 3 × 3 CA partitioning was chosen for the inverse modeling with the same initial parameterized model than in study cases 4 and 5. The covariance matrices  $C_{\beta}$  were generated with a seismic velocity variance of  $\sigma_{\beta}^2 = 1$  km/s and a multiplicative variance on the transmissivity of the form  $10^{\pm\sigma_{\beta}^2}$  where  $\sigma_{\beta}^2 = 1$  ( $\pm 1$  variance on the transmissivity exponent), and the seismic velocities and hydraulic transmissivities of the initial models were also taken as prior values in  $P_{\beta, \text{prior}}$ .

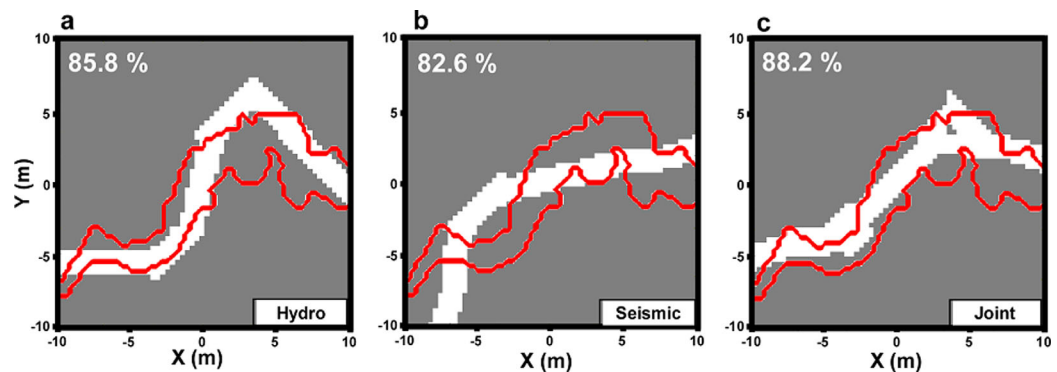


**Figure 16.** Pixel-wise comparison of the optimal structures found by inversion (in white) and the true structure (bold boundaries) for the study cases (a) 4, (b) 5, and (c) 6. Both hydraulic and seismic data permitted to find a geometry of the global trends of the true structure but the joint inversion resulted to a better model regarding the structure and also the convergence on the data, which avoided the difficulties encountered by the simple hydraulic inversion and the simple seismic inversion.

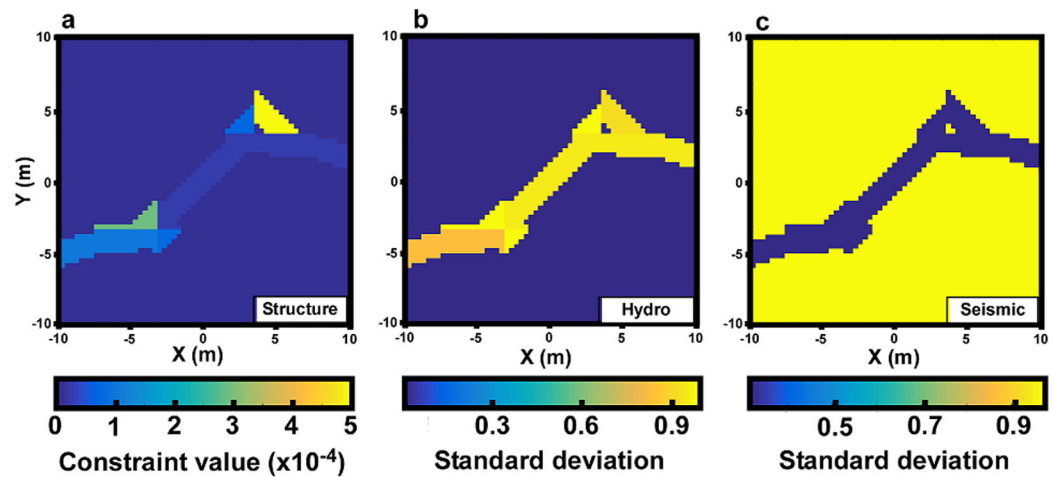


**Figure 17.** Uncertainties analysis for the joint inversion of the study case 6. The structural constraint in (a) indicates where the structure of the model is well-constrained by a low value, and at the opposite, a high value indicates an uncertainty for its subspace direction. The properties uncertainties for (b) the hydraulic transmissivity and (c) the seismic velocity are quantified by a standard deviation on the inverted values.

The inversion converged in seven iterations. The results of the inversion for each method and the true models are presented in Figure 15. Compared to the hydraulic and seismic separate inversion, the joint inversion produced better results on the data (Table 1) and on the inverted structure (Figure 16) which is closer to the true structure. The structural joint inversion permits to combine the hydraulic and seismic data to find the best structure. The optimized property values are also better in the joint inversion than in the separate ones. The properties optimization permits to counterbalance the limitations of a constant aperture structure by keeping a modeled higher value of transmissivity for the structure regarding the true value to simulate a thicker structure. The lower left part of the structure was optimized with a transmissivity close to the real one because the true structure is thinner in this part. The seismic velocity of the structure was also kept at a lower value than the true one to counterbalance to constant aperture geometry.

The uncertainties analysis on the structure and the property values are reported in Figure 17. The structure is well constrained by the data, except in the lower left part where the true structure is thinner and the upper right part for the angle of the structure. This means that another close subdirection of the inverted structure would not affect significantly the results. In the parameterization of the joint inversion more accuracy was given to the hydraulic data, therefore the uncertainties on the seismic properties are more important than those on the hydraulic ones. The uncertainties on the hydraulic property values vary locally within the structure. The lower left part has fewer uncertainties on the properties because its aperture is closer to the true one and therefore this part is globally closer to the true structure. The background value is well constrained because the true value was considered as a priori known. The seismic properties uncertainties

**Table 2.** Main Advantages Provided by the CADI Algorithm<sup>a</sup>

Advantages	Limits	Solutions
<ol style="list-style-type: none"> <li>1. The complexity of the structural optimization can be monitored with a configurable partitioning of the model</li> <li>2. The model properties are monitored by pilot cellular automaton, which permits to easily handle with large-scale modeling and makes a sensitivity analysis possible to accelerate the optimization</li> <li>3. The convergence of the inversion is constraint to a local solution regarding the prior information which can be easily incorporated in the objective function</li> </ol>	<ol style="list-style-type: none"> <li>1. The cellular automata parameterization permits only the formation of structure with a constant aperture all along in the structural optimization</li> <li>2. Only binary pattern are considered (structure and background). The background is considered as invariable regarding the variation structure/background and intrastructure</li> </ol>	<ol style="list-style-type: none"> <li>1. The property values optimization permits to digitally balance some local variation of aperture. Thus, some results on property values can be structurally interpreted</li> <li>2. If the algorithm is applied on a case where the background has significant intern variability, a particular attention should be paid on setting an appropriate equivalent background</li> </ol>

<sup>a</sup>The limits of the methods are also listed with a suggested solution for each limit.

are more important for its background. This is caused by the high properties difference between structure and background and because the background property was initially not known.

### 5. Discussion and Conclusion

The Cellular Automata-based Deterministic Inversion (CADI) algorithm is an especially adapted method for linear structure geometries. The inversion process is based on a Bayesian approach and a sequentially optimization of the structure geometry and property values. The structural optimization is monitored by cellular automaton to generate the structure, and by a configurable partitioning of the model into subspaces which permits a monitoring of the complexity of the inverted structure. One can choose a coarse subspace partitioning for simple structures and for a fast inversion process, or a fine subspace partitioning for inversion of more complex structures. The property values optimization brings more flexibility to the inversion by slightly modifying the values of the properties in the structure. This optimization permits to counterbalance some approximations in the structural optimization and some constraints from the initial information.

The CADI algorithm parameterization is mainly focused on the structural optimization, therefore it considers only two units: a constant-aperture structure and a background, which is considered as a unique uniform unit or with an intern variability which is negligible regarding the variability with the structure. Therefore, and as for any other inversion methods, it is especially effective for specific structural cases. Furthermore, the limits of the CADI algorithm have to be clearly identified in order to make a good use out of it and to have a critical view on the results it can produce. For this purpose, the main advantages and limits of the CADI algorithm have been summarized in Table 2. For each limit of the algorithm, an appropriate solution has been suggested.

In this paper we promote the potential of the CADI algorithm to image the complex linear structures, exploiting its capacity to reproduce large-scale structures in a relatively short time. As far as we know, the CADI algorithm is the first algorithm which permits the deterministic inversion of linear structures (global direction-oriented structure characterized by an aperture significantly lower than its length) with a dynamic structural optimization. This first attempt is mainly focused on the general presentation of the method and the theory of the algorithm, but we believe that this method can be improved and inspire other ones in various domain. For example, with the same algorithm structure, and by changing the cellular automaton configuration rules, it is conceivable to generate other types of forms than linear structures. We also plan further works with the presented algorithm, especially for improvements on its capacities (by adding a third "microstructures" state within the background) and for field application cases, with a higher consideration on additional prior information (as the tortuosity factor of the structure) and on sensitivity analysis of the method.

### Appendix A

This appendix contains Figure A1.

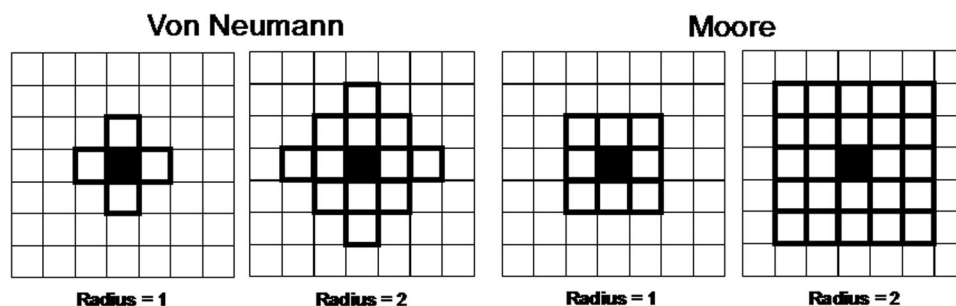


**Figure A1.** Two mainly used CA neighborhood definition. The two left configuration represent a Von Neumann neighborhood and the two right configuration represent a Moore neighborhood. These neighborhoods are presented for their first two radiuses. The black-filled cell is the cell under consideration during the CA process, and the black highlighted cells are the cells considered as its neighbors in the transition rule.

### Acknowledgments

We would like to thank three anonymous reviewers for their relevant comments which permitted to significantly improve the quality of this article. We also thank the region Normandy for financially supporting the PhD of Pierre Fischer. The data and codes used to produce the results of this paper can be obtained from the first or second author.

### References

- Bruna, P.-O., Y. Guglielmi, S. Viseur, J. Lamarche, and O. Bildstein (2015), Coupling fracture facies with in-situ permeability measurements to generate stochastic simulations of tight carbonate aquifer properties: Example from the lower cretaceous aquifer, Northern Provence, SE France, *J. Hydrol.*, *529*, 737–753.
- Cardiff, M., and P. K. Kitanidis (2009), Bayesian inversion for facies detection: An extensible level set framework, *Water Resour. Res.*, *45*, W10416, doi:10.1029/2008WR007675.
- Chopard, B., and A. Masselot (1999), Cellular automata and lattice Boltzmann methods: A new approach to computational fluid dynamics and particle transport, *Future Gener. Comput. Syst.*, *16*, 249–257.
- Dewri, R., and N. Chakraborti (2005), Simulating recrystallization through cellular automata and genetic algorithms, *Modell. Simul. Mater. Sci. Eng.*, *13*(2), 173–183.
- Gallardo, L. A., and M. A. Meju (2011), Structure-coupled multiphysics imaging in geophysical sciences, *Rev. Geophys.*, *49*, RG1003, doi: 10.1029/2010RG000330.
- Ghosh, S., P. Gabane, A. Bose, and N. Chakraborti (2009), Modeling of recrystallization in cold rolled copper using inverse cellular automata and genetic algorithms, *Comput. Mater. Sci.*, *45*, 96–103.
- Grimstad, A.-A., T. Mannseth, G. Naevdal, and H. Urkedal (2003), Adaptive multiscale permeability estimation, *Comput. Geosci.*, *7*(1), 1–25.
- Haber, E., and D. Oldenburg (1997), Joint inversion: A structural approach, *Inverse Problems*, *13*, 63–77.
- Halder, C., L. Madej, and M. Pietrzyk (2014), Discrete micro-scale cellular automata model for modelling phase transformation during heating of dual phase steels, *Arch. Civ. Mech. Eng.*, *14*, 96–103.
- Halder, C., D. Bachniak, L. Madej, N. Chakraborti, and M. Pietrzyk (2015), Sensitivity analysis of the finite difference 2-D cellular automata model for phase transformation during heating, *J. Iron Steel Inst. Jpn.*, *55*(1), 285–292.
- Hale, D. (2009), Structure-oriented smoothing and semblance, *CWP Rep. 635*, Cent. for Wave Phenomena. [Available at <http://inside.mines.edu/~dhale/papers/Hale09StructureOrientedSmoothingAndSemblance.pdf>.]
- Hoeksema, R. J., and P. K. Kitanidis (1984), An application of the geostatistical approach to the inverse problem in two-dimensional ground-water modeling, *Water Resour. Res.*, *20*(7), 1003–1020.
- Jafarpour, B., V. K. Goyal, D. B. McLaughlin, and W. T. Freeman (2010), Compressed history matching: Exploiting transform-domain sparsity for regularization of nonlinear dynamic data integration problems, *Math. Geosci.*, *42*, 1–27.
- Javadi, M., M. Sharfzadeh, and K. Shahriar (2016), Uncertainty analysis of groundwater inflow into underground excavations by stochastic discontinuum method: Case study of Siah Bisheh pumped storage project, Iran, *Tunnelling Underground Space Technol.*, *51*, 424–438.
- Jin, Z., and Z. Cui (2012), Investigation on dynamic recrystallization using a modified cellular automaton, *Comput. Mater. Sci.*, *63*, 249–255.
- Lee, J., and P. K. Kitanidis (2013), Bayesian inversion with total variation prior for discrete geologic structure identification, *Water Resour. Res.*, *49*, 7658–7669.
- Lelièvre, P. G., and D. W. Oldenburg (2009), A comprehensive study of including structural orientation information in geophysical inversions, *Geophys. J. Int.*, *178*, 623–637.
- Lochbühler, T., J. A. Vrugt, M. Sadegh, and N. Linde (2015), Summary statistics from training images as prior information in probabilistic inversion, *Geophys. J. Int.*, *201*, 157–171.
- Lu, Z., and B. A. Robinson (2006), Parameter identification using the level set method, *Geophys. Res. Lett.*, *33*, L06404, doi:10.1029/2005GL025541.
- Moore, E. F. (1962), Machine models of self-reproduction, *Am. Math. Soc.*, *14*, 17–33.
- Pan, P.-Z., X.-T. Feng, D.-P. Xu, L.-F. Shen, and J.-B. Yang (2011), Modelling fluid flow through a single fracture with different contacts using cellular automata, *Comput. Geotech.*, *38*, 959–969.
- Pardo-Igúzquiza, E., P. A. Dowd, C. Xu, and J. J. Durán-Valsero (2012), Stochastic simulation of karst conduit networks, *Adv. Water Resour.*, *35*, 141–150.
- Reeves, D. M., R. Parashar, G. Pohll, R. Carroll, T. Badger, and K. Willoughby (2013), The use of discrete fracture network simulations in the design of horizontal hillslope drainage networks in fractured rock, *Eng. Geol.*, *163*, 132–143.
- Soueid Ahmed, A., J. Zhou, A. Jardani, A. Revil, and J. P. Dupont (2015), Image-guided inversion in steady-state hydraulic tomography, *Adv. Water Resour.*, *82*, 83–97.
- Sun, X., P. L. Rosin, and R. R. Martin (2011), Fast rule identification and neighbourhood selection for cellular automata, *IEEE Trans. Syst. Man Cybern. Part B, Cybern.*, *41*(3), 749–760.
- Tan, S. K., and S.-U. Guan (2007), Evolving cellular automata to generate nonlinear sequences with desirable properties, *Appl. Soft Comput.*, *7*, 1131–1134.
- Tarantola, A., and B. Valette (1982), Generalized nonlinear inverse problems solved using the least squares criterion, *Rev. Geophys. Space Phys.*, *20*(2), 219–232.
- Tsai, F. T.-C., N.-Z. Sun, and W. W.-G. Yeh (2003), Global-local optimization for parameter structure identification in three-dimensional groundwater modeling, *Water Resour. Res.*, *39*(2), 1043, doi:10.1029/2001WR001135.
- Van der Weeën, P., J. M. Baetens, and B. de Baets (2011), Design and parameterization of a stochastic cellular automaton describing a chemical reaction, *J. Comput. Chem.*, *32*, 1952–1961.
- Von Neumann, J., and A. W. Burks (1966), *Theory of Self-Reproducing Automata*, Univ. of Ill. Press. [Available at <http://cba.mit.edu/events/03.11.ASE/docs/VonNeumann.pdf>.]